Catalysis Communications 186 (2024) 106833

Contents lists available at ScienceDirect

Catalysis Communications

journal homepage: www.elsevier.com/locate/catcom

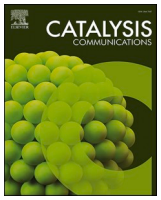

Investigation of catalytic activation of peroxydisulfate on cu-doped mesoporous silica-based particles (Cu-BMS) for efficient degradation of methylene blue

Saeed Sajjadi [a,*], Akrity Anand [a], Ana M. Beltrán [b], Dana Dvoranová [c], Aldo R. Boccaccini [d], Dagmar Galusková [a], David Jaška [e], Róbert Klement [a,*]

[a] Centre for Functional and Surface Functionalized Glass, Alexander Dubček University of Trenčín, Trenčín 911 50, Slovakia
[b] Departamento de Ingeniería y Ciencia de Los Materiales y Del Transporte, Universidad de Sevilla, Escuela Politécnica Superior, Virgen de África 7, Seville 41011, Spain
[c] Institute of Physical Chemistry and Chemical Physics, Faculty of Chemical and Food Technology, Slovak University of Technology in Bratislava, Radlinského 9, Bratislava SK-812 37, Slovakia
[d] Institute of Biomaterials, University of Erlangen-Nuremberg, Erlangen 91058, Germany
[e] Department of Polymer Engineering, Faculty of Technology, Tomas Bata University in Zlín, Vavrečkova 5669, 760 01 Zlín, Czech Republic

ARTICLE INFO

Keywords:
Mesoporous catalyst
Persulfate activation
Advanced oxidation process (AOP)
Organic pollutant

ABSTRACT

The Cu-doped mesoporous silica-based particles (Cu-BMS) were prepared using an evaporation-induced self-assembly sol-gel procedure as a heterogeneous catalyst for the activation of peroxydisulfate (PDS). The formation of well-organized mesoporous structures with amorphous nature and high surface area of 286 m^2/g was demonstrated. The catalytic activity of Cu-BMS in the degradation of Methylene Blue (MB) and the effects of operating parameters, including Cu-BMS dosage, initial PDS amount, initial MB concentration, temperature and initial pH, were investigated in details. The Cu-BMS demonstrated a remarkable catalytic activity (93.5% degradation efficiency within 60 min) and good stability.

1. Introduction

Large volumes of organic pollutants have been released by the rapidly developing chemical sector, posing major risks to the environment and public health. The presence of dyes in industrial wastewater from the textile industry is a major concern in developing regions, mainly due to the presence of various persistent pollutants. The textile industry's daily consumption of freshwater is a significant concern, given the vast range of over 100,000 possible colors worldwide. Methylene blue (MB) is a common color found in textile effluent, along with other dye compounds. This particular basic dye, based on thiazine, has the ability to cause long-term environmental damage by blocking sunlight in water bodies, thereby affecting the aquatic ecosystem and its inhabitants. From a public health perspective, it should be noted that MB can cause ocular burns, which may lead to lasting injury. When ingested, this substance causes a feeling of intense heat, resulting in the expulsion of stomach contents through vomiting [1,2].

Advanced oxidation processes (AOPs) have been widely demonstrated as promising technologies for environmental remediation. AOPs can generate reactive oxygen species (ROS) to degrade organic contaminants into smaller molecules or water and carbon dioxide [3–6]. Traditional oxidants, such as hydrogen peroxide (H_2O_2), can be converted into hydroxyl radicals ($^{\bullet}OH$, $E^0 = 1.89–2.72$ V vs. NHE) by iron ions (Fe^{2+}) and are used in AOPs. However, this system cannot be applied on a large scale because it produces a large amount of sludge and works only within a narrow pH range (2–3). In recent decades, extensive research has been conducted on the sulfate radical ($SO_4^{\bullet-}$, $E^0 = 2.5–3.1$ V vs. NHE)-based AOPs, which are viable alternatives [7,8]. In a wide pH range (3–9), persulfates, such as peroxymonosulfate (PMS, $E^0 = 1.4$ V vs. NHE) and peroxydisulfate (PDS, $E^0 = 2.01$ V vs. NHE), are stable solid oxidants with excellent AOP efficiency. PDS has longer O–O bonds than PMS, which makes it easier to activate and shows better oxidation capacity in the commercial oxidation process. Moreover, AOP based on PDS provide the benefits of low sludge output and gentle working conditions. It has been previously stated that sulfate radicals can be generated via ultraviolet (UV) light, heat, ultrasound (US), and transition metals, according to Eqs. (1–3) [9–11].

* Corresponding authors.
E-mail addresses: mir.sajjadi@tnuni.sk (S. Sajjadi), robert.klement@tnuni.sk (R. Klement).

https://doi.org/10.1016/j.catcom.2023.106833
Received 9 October 2023; Received in revised form 11 December 2023; Accepted 25 December 2023
Available online 28 December 2023

$$S_2O_8^{2-} \xrightarrow{heat} 2SO_4^{\bullet -} \quad (1)$$

$$S_2O_8^{2-} \xrightarrow{US\ or\ UV} 2SO_4^{\bullet -} \quad (2)$$

$$S_2O_8^{2-} + M^{n+}(Metal) \rightarrow SO_4^{2-} + SO_4^{\bullet -} + M^{(n+1)+} \quad (3)$$

Among these, homogeneous systems with transition metal ions (Fe^{2+}, Cu^{2+}, Mn^{2+}, Co^{2+}, etc.) are regarded as the most effective. Recent studies have demonstrated that copper is better than other transition metals for catalyzing chemical reactions, particularly in the efficient activation of PDS [12] and PMS [13], using a wider range of methods [14]. Cu-based catalysts can activate both PMS and PDS to produce free radicals (like $SO4^{\bullet -}$, $^{\bullet}OH$, and $O_2^{\bullet -}$), singlet oxygen ($^1O_2$), and Cu(III) [15–17]. Nevertheless, homogeneous catalysts have the drawback of being difficult to recover and prone to causing secondary pollution throughout the wastewater treatment process [18]. Compared to homogeneous systems, heterogeneous catalysts such as metals, metal oxides, and supported metal oxides have less environmental impact and are more recyclable [8].

In recent years, numerous research efforts have been made to increase the generation rate of activated species and accelerate reaction kinetics to maximize the efficiency of organic compound degradation. In particular, catalysts based on Cu, which have the benefits of variable valence, abundant active sites, and high surface reactivity, have been the subject of intense research because of their potential to efficiently degrade organic pollutants [14,19]. Mesoporous silicas, such as SBA-15 (Santa Barbara Amorphous-15, a mesoporous silica sieve), are frequently used as support matrices for heterogeneous Cu-based catalysts owing to their large surface area, thermal stability, flexibility for chemical modification, and environmental friendliness [20–23]. Only a few studies have been conducted on the catalytic effectiveness of well-dispersed Cu species supported on mesoporous silica for AOP [24–27]. Mesoporous silica SBA-15 catalysts containing Cu nanoparticles have shown excellent catalytic activity for the reduction of different dyes [28].

The main aim of this study was to investigate the catalytic activation of PDS using Cu-doped mesoporous silica-based particles (Cu-BMS, SiO_2-CaO-CuO-P_2O_5) for the degradation of MB, a typical organic dye in wastewater. Cu-BMS was prepared through the sol-gel method. The effects of the operating parameters, including Cu-BMS dosage, initial PDS amount, initial MB concentration, and initial pH, were investigated. Quenching tests were also conducted to determine the participation of the reactive radical species in the degradation process. Finally, the stability of the Cu-BMS was evaluated using 12 repetitive runs. To the best of our knowledge, this is the first investigation on the catalytic activity of Cu-doped mesoporous silica particles as a heterogeneous catalyst for PDS activation.

2. Materials and methods

2.1. Preparation of Cu-BMS

Cu-BMS, with a composition of 80% SiO_2, 11% CaO, 4% CuO, and 5% P_2O_5 (mol%), was prepared using an evaporation-induced self-assembly (EISA) sol-gel procedure [29]. In a typical procedure, 0.875 mL of hydrochloric acid (HCl, 0.5 mol/L, Merck, Germany) was mixed with 79.84 mL of ethanol (Mikrochem, Slovakia), and the resulting solution was mixed with 4.2 g of Pluronic® P-123 (Poly(ethylene glycol)-poly (propylene glycol)-poly(ethylene glycol), M_n = 5800, Merck, Germany). In addition, 8.25 mL of tetraethyl orthosilicate (TEOS, ~98.0%, Merck, Germany), 0.78 mL of triethyl phosphate (TEP, ~99.8%, Merck, Germany), 1.2 g of calcium nitrate tetrahydrate ($Ca(NO_3)_2.4H_2O$, ~99%, VWR International GmbH, United States), and 0.248 g of copper (II) chloride ($CuCl_2$, ~99%, Merck, Germany) were dissolved in the above solution. At 32 °C and 75% humidity, the prepared sol was cast into Petri dishes (100 mm × 20 mm) for the EISA process. The EISA process took place over approximately nine days. To obtain Cu-BMS particles, the final gel was calcined at 700 °C (2 °C/min) for 5 h.

2.2. Characterization

Powder X-ray diffraction (XRD) patterns of the as-prepared Cu-BMS particles were recorded on an X-ray diffractometer (Empyrean, Malvern Panalytical, Almelo, Netherlands) using Cu-K_α (1.54184 Å) radiation at 45 kV and 40 mA. The presence of a mesoporous structure was verified using the small-angle X-ray scattering (SAXS) technique. The measurement was conducted using an Anton Paar SAXSpace instrument, employing Cu-K_α (1.54184 Å) radiation at 40 kV and 50 mA, in line collimation mode. The sample and detector were separated by a distance of 307 mm, and the exposure time was 3 min. The sample surface was inspected by X-ray Photoelectron Spectroscopy (XPS) using Nexsa G2 XPS Surface Analysis System (Thermo Scientific). The microstructure of the Cu-BMS particles was examined using a JSM-7600F scanning electron microscope (SEM, Jeol, Japan). To prove the mesoporous structure of prepared particles and the presence of the mentioned elements in the structure, transmission electron microscopy (TEM) and energy-dispersive X-ray spectroscopy (EDX) were carried out using a Talos F200X system (Thermo Fisher Scientific, USA); an accelerating voltage of 200 kV was applied for imaging. Optical emission spectrometry with inductively coupled plasma (ICP-OES, Agilent 5100 SVDV, USA) was used to analyze the chemical composition of the Cu-BMS particles. The sample for analysis was prepared by dissolving 25 mg of Cu-BMS in a solution containing 6 mL of 30% hydrochloric acid (30%, Merck), 2 mL of nitric acid (67–69%, Analytika Ltd.), and 0.5 mL of hydrofluoric acid (47%, VWRchemicals). After the complete dissolution of the sample, the resulting solution was analyzed using ICP-OES. To determine the possible leaching of Cu ions from the Cu-BMS particles into the aqueous solution, a leaching test was performed using the following procedure. The amount of Cu ions released into the solution during the reaction was analyzed using ICP-OES. After completing the degradation process, a 10 mL sample of the solution was collected, and the catalyst was separated by centrifugation. Subsequently, two drops of concentrated nitric acid (68%) were introduced into the sample to reach pH < 2 and keep analyte in dissolved form prior the analysis. In the ICP-OES measurement, the carrier gas flow, wavelength, and radiofrequency power were 0.55 L/min, 327.395 nm, and 1.2 kW, respectively.

Infrared (IR) spectra were recorded using Fourier-transform infrared (FTIR) spectrometer IRAffinity-1S (scan speed:40 scans/min, resolution:4 cm^{-1}, SHIMADZU, Japan). The pore volume and Brunauer–Emmett–Teller (BET) surface area were determined using a Belsorp-mini II analyzer (Microtrac, Japan). A simultaneous thermal analyzer (STA 449F1, Netzsch, Germany) was used for thermal analyses (DTA and TGA) of the Cu-BMS particles. These analyses were performed at a standard heating rate of 10 K/min up to 1000 °C in air atmosphere.

The EPR experiments at room temperature (295 K) with dispersed systems in deionized water under air atmosphere were carried out employing EPR spectrometer (Bruker, Germany) operating in X-band at 100 kHz field modulation in the TM resonator (Bruker) with the small quartz flat cell (WG 808-Q, Wilmad-LabGlass, optical cell length 0.045 cm). The spin trapping agent 5,5-dimethyl-1-pyrroline N-oxide (DMPO, Sigma-Aldrich) was distilled before application and stored at −18 °C. The 4-oxo-2,2,6,6-tetramethylpiperidone (TMPO, Sigma-Aldrich) was used as supplied. The 50 μL DMPO (0.212 M stock solution in deionized water) was added to the reaction suspension containing 100 μL of Cu-BMS suspension (1.0 g/L) and 100 μL of PDS solution (4 g/L), i.e. similar concentrations as in experiments of Cu-BMS catalytic activity assessment. The reaction mixture was transferred into quartz flat cell and the EPR spectra were recorded in situ. The EPR spectra acquisition started 3 or 11 min after mixing. For comparison, the experiment at the same conditions was conducted without the Cu-BMS catalyst; the 50 μL DMPO (0.212 M stock solution in deionized water) was added into the

mixture of 100 μL of PDS solution (4 g/L) diluted with 100 μL of deionized water. The relative concentration of paramagnetic species was evaluated from the double-integrated EPR spectra. The experimental EPR spectra were analyzed using WinEPR software (Bruker) and the calculations of spin Hamiltonian parameters and relative concentrations of individual spin adducts were performed with the EasySpin toolbox working on MatLab® platform [30].

2.3. Catalytic activity assessment

The catalytic activity of Cu-BMS for PDS activation was evaluated based on the degradation of MB. The degradation process was carried out in a 250 mL Pyrex beaker under magnetic stirring at 25 °C. According to commonly used methodology [31,32], a specific quantity of sodium persulfate ($Na_2S_2O_8$, 99%, Merck, Germany) was added to 100 mL of MB solution (100 mg/L). The catalytic degradation process was initiated by adding a defined amount (0.05, 0.1, 0.2, 0.3, and 0.4 g) of Cu-BMS. To follow the MB degradation kinetics, 3 mL of the reaction solution was collected at regular intervals (every 10 min) during the degradation process, and the catalyst was separated by centrifugation. The concentration of MB in the solution was determined spectrophotometrically using a UV–Vis-NIR spectrophotometer (Cary 5000, Agilent, United States). The effects of the operating parameters, including the Cu-BMS dosage, initial amount of PDS, initial MB concentration, initial pH, and radical species scavengers, on the degradation efficiency (DE%) were studied. DE% of the MB was determined using the Eq. (4) [33]:

$$DE\% = \left(1 - \frac{A_t}{A_0}\right) \times 100 \quad (4)$$

where A_0 and A_t are the initial absorbance and absorbance at a particular time in the process (t, min), respectively. The stability of the Cu-BMS catalyst was investigated by collecting, washing (with isopropanol and deionized water), and drying (overnight at 100 °C) the catalyst after each degradation step.

3. Results and discussion

3.1. Cu-BMS characterization

The transformation temperatures and mass losses of the Cu-BMS sample prior to calcination at 700 °C for 5 h were determined by DTA-TGA analysis. Fig. 1a shows the DTA-TGA thermograms of the Cu-BMS prepared with the Pluronic® P-123 surfactant. Because the sol-gel EISA process was carried out under high-humidity conditions and a surfactant was present, additional weight loss was expected. During heating to 1000 °C, three exothermic peaks were observed in the DTA curve at approximately 66–104, 127–201, and 250–470 °C. The first two peaks, which appeared below 201 °C, were linked to the release of adsorbed water molecules from the surface, resulting in a weight loss of 11%. A weight loss of up to 55% was measured between 250 and 470 °C, which can be attributed to the decomposition of the remaining nitrate and burning of the residual surfactant. Burning of the surfactant may release a significant amount of CO_2 and H_2O, resulting in a broad

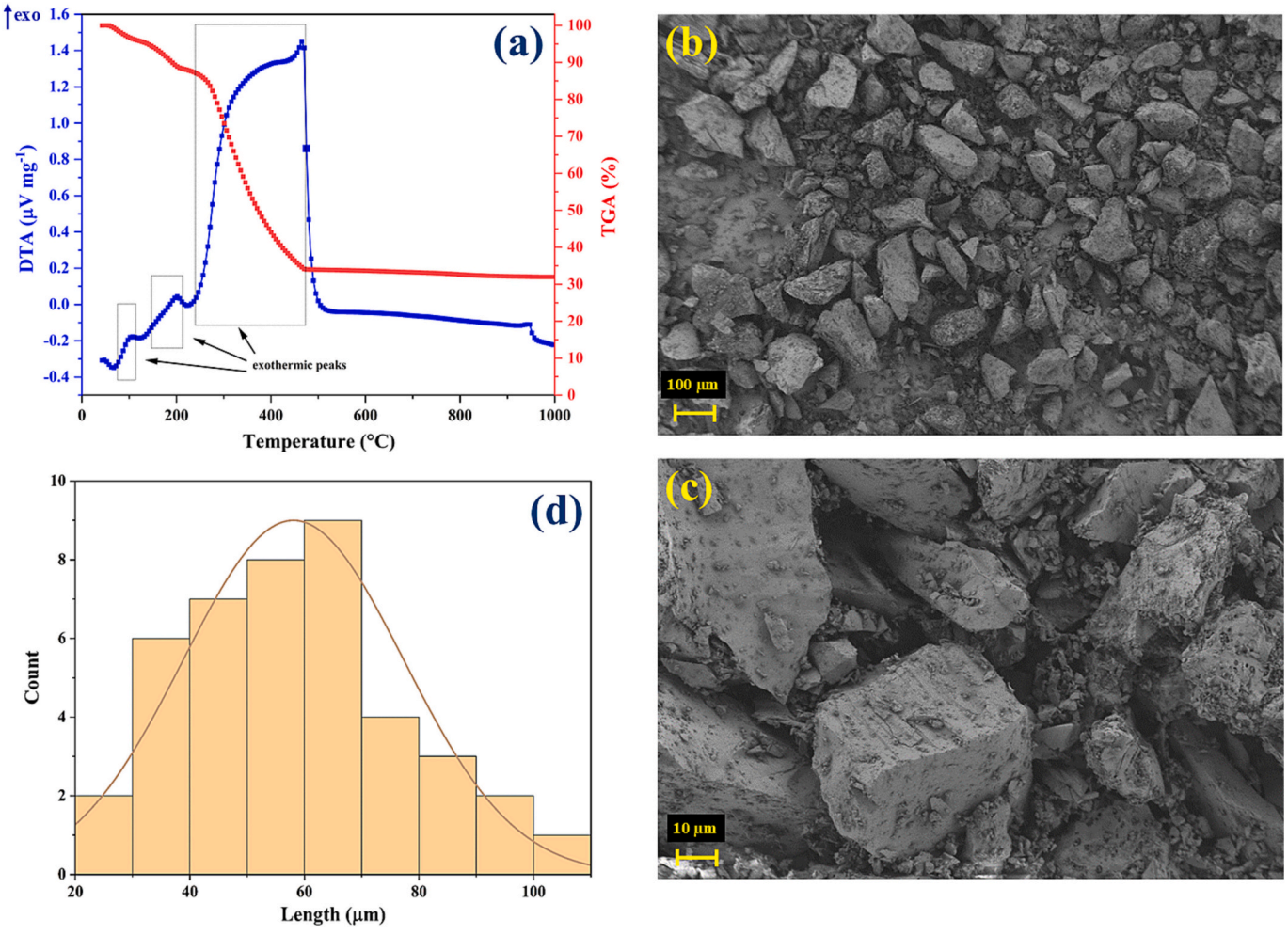

Fig. 1. (a) DTA-TGA thermograms, (b, c) SEM images, and (d) particle size distribution histogram of Cu-BMS particles prior to calcination at 700 °C for 5 h.

exothermic peak [34,35]. Based on the DTA-TGA analysis, 700 °C was selected for calcination to obtain mesoporous Cu-BMS particles.

According to the SEM images (Fig. 1b, c) of the as-prepared Cu-BMS particles, the final particles exhibited a polygonal shape, with smaller particles adhering to larger particles. From the SEM images using ImageJ (National Institutes of Health, MD, USA) and applying the Gaussian distribution function, the average particle size was estimated to be 58 ± 19 μm (Fig. 1d).

The XRD pattern obtained from the as-prepared Cu-BMS particles (Fig. 2a) reveals the amorphous nature of the Cu-BMS particles, which is documented by the amorphous halo that appears from 15° to 36° 2θ, which is typical for amorphous systems, such as silicate glasses [36]. Furthermore, the presence of hints of peaks at specific 2θ values, namely 32.5°, 35.5°, 38.8°, and 48.8°, which correspond to the crystalline planes of (110), (002), (111), and (202) respectively, provides evidence for the creation of CuO (JCPDS-01–089-5899) [37] within the structure of BMS. The low intensity of the CuO peaks in XRD trace could be attributed to the low loading and highly dispersed nature of the copper species within the mesoporous silica structure, which might result in low crystallinity or small crystal sizes. It is also reasonable to expect, that copper ions can be bounded to non-bonding oxygens within the amorphous structure/framework of the BMS. Additionally, the small-angle X-ray diffraction analysis was performed, and the result is illustrated in Fig. 2a (inset). A distinct diffraction peak at 1.2° is evident, corresponding to the reflections of the 100 plane. Two minor peaks at 1.75° and 2.03° were also observed, and identified as the reflection of the 110 and 200 planes [38]. The reflections confirmed the presence of a mesoporous structure, which closely match the findings of the TEM examination.

To gain a better understanding of the characteristics of the copper species in Cu-MBS, XPS analysis was conducted. According to the XPS survey results (Fig. S1, Supplementary Material), O, Si, P, Ca, and Cu elements were detected. The presence of the C peak in the XPS survey is due to impurities that were absorbed during storage and analysis. The peak fit of Cu 2p core level XPS spectrum is shown in Fig. 2b. The peaks located at 936.8 and 955.9 eV can be attributed to the Cu(II) state, whereas the peaks positioned at the binding energy values of 934.4 and 953.3 eV are assigned to the Cu(I) state. The satellite peaks, as usually observed for copper, at around 944 and 963 eV can be attributed to the shake-up phenomenon, which arises as a consequence of the unoccupied 3d orbital of Cu(II) [39]. It is worth noting that the presence of Cu(I) in the Cu-BMS benefits the PDS activation process [40].

The FTIR spectrum of Cu-BMS (Fig. 2c) revealed that all organic compounds used in the preparation were removed after heat treatment at 700 °C for 5 h. The bands around 450 and 800 cm^{-1} can be assigned to Si-O-Si symmetric vibrations, and the band located at 1060 cm^{-1} can be

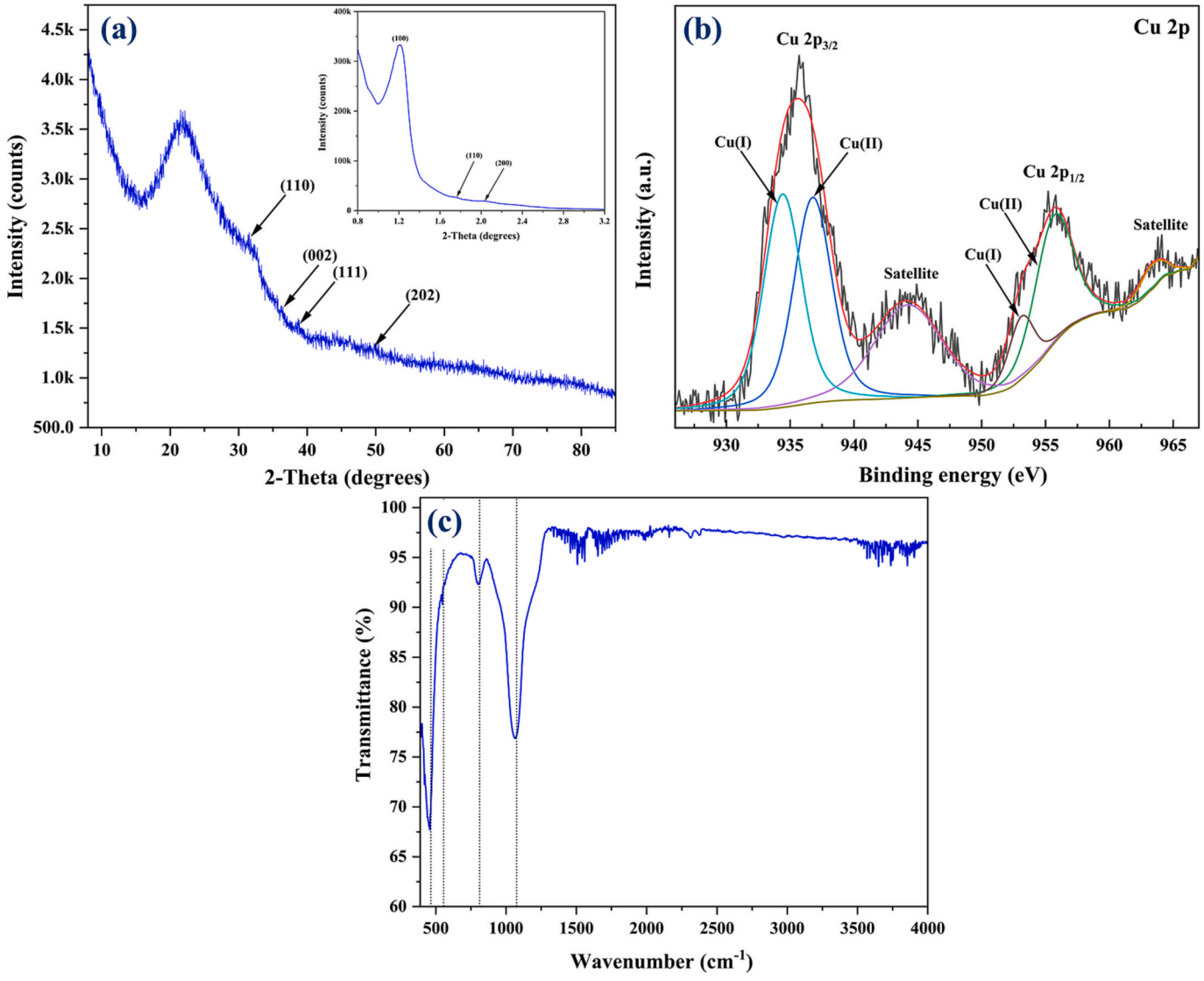

Fig. 2. (a) XRD pattern (the inset represents the Small-angle XRD pattern), (b) Cu 2p high-resolution XPS spectra, and (c) FT-IR spectrum of Cu-BMS particles.

ascribed to the Si-O-Si anti-symmetric stretching mode. Moreover, this spectrum exhibited a very low-intensity peak at approximately 540 cm^{-1}, which was assigned to the vibrations of P–O in calcium phosphates [41,42].

The chemical composition of the Cu-BMS particles was determined using ICP-OES (after sample decomposition) and EDX analyses. Based on ICP-OES analysis of the Cu-BMS sample, Table 1 lists its composition and standard deviation. Silica-based compounds dissolve in hydrofluoric acid (HF) by breaking strong Si–O bonds and forming hexafluorosilicic acid ($H_2[SiF_6]$), which exists in its dissociated form (SiF_6^{2-}) in water. Owing to the high SiO_2 content (80 mol%) of Cu-BMS, the partial formation of volatile silicon tetrafluoride (SiF_4) cannot be excluded, which could result in Si loss during decomposition. Therefore, this method cannot provide complete recovery for silicon analysis, and the values for SiO_2 present in Cu-BMS were estimated by normalizing it to 100%. Although the presence of Cu was confirmed by ICP-OES analysis, the actual composition of the prepared sample differed from the nominal composition, especially in terms of the amount of phosphorus, which was significantly lower than expected. This discrepancy can be attributed to the different hydrolysis rates of the two precursors (TEP and TEOS) under acidic pH conditions during preparation. Specifically, the rapid hydrolysis of TEOS and condensation of SiO_2 particles, compared to TEP, prevents the incorporation of PO_4 structural units into the amorphous SiO_2 structural network, thus leading to a reduced level of P_2O_5 in the Cu-BMS system [43]. The remaining P_2O_5 may act as a network former and form bonds with silica and calcium [44]. Additionally, EDX analysis confirmed the high purity of the synthesized Cu-BMS particles by detecting Si, Ca, P, O, and Cu in their structures without the presence of other unwanted elements (Table 1).

TEM images of the specimen confirmed the existence of a well-ordered, cylindrical-like mesoporous structure (Fig. 3a). Mesoporous structures are formed as a result of the regular packing (self-assembly) of micelles and homogenous distribution of organic–inorganic species [45]. The study employed an optimized amount of surfactant to achieve homogenization of inorganic-organic pairs. This approach ensures that the formation of ordered mesopores is not interrupted by any additional surfactant species. Moreover, the EISA method was utilized to condense inorganic species, and control of temperature and humidity led to an organized mesoporous structure within the Cu-BMS particles [46].

N_2 adsorption–desorption analysis was performed to investigate the pore structure and BET surface area. The Cu-BMS exhibited a type-IV curve with an H1 hysteresis loop according to the IUPAC classification [47], as shown in Fig. 3b. The H1 hysteresis loop confirms the formation of narrow distribution of uniform cylindrical mesoporous structures which is open at both ends [48]. Based on the multipoint BET method, the Cu-BMS particles have a large specific surface area ($a_{s,BET}$) of 286.94 m^2/g. This mesoporous structure was further confirmed using the Barrett-Joyner-Halenda method [49], which determined an average pore size of 5.54 nm. The total pore volume and monolayer adsorption amount (V_m) of the Cu-BMS were 0.3976 cm^3/g and 65.926 cm^3(STP)/g, respectively.

Table 1
ICP-OES and EDX-TEM data of Cu-BMS particles.

ICP-OES				
	SiO_2	CaO	P_2O_5	CuO
Nominal composition (Wt%)	**74.50**	**9.56**	**11**	**4.93**
Actual composition (ICP-OES) (Wt%)	**77.6 ± 0.6**	**11.2 ± 0.5**	**1.5 ± 0.6**	**5.3 ± 0.2**
EDX-TEM				
Element	Wt%		At.%	
Cu	**5.80**		**1.93**	
O	**49.66**		**65.79**	
Si	**38.11**		**28.76**	
P	**0.72**		**0.49**	
Ca	**5.68**		**3.00**	

3.2. Catalytic activity of Cu-BMS catalyst

A comparison of the degradation of MB by different systems, including Cu-BMS/PDS, Cu^{2+}/PDS, Cu-BMS (adsorption), and PDS, is shown in Fig. 4a. The insignificant DE% (<13%) within 60 min indicates that inactivated PDS alone cannot result in high degradation of MB, which is in accordance with previous reports [50–52]. Additionally, the DE% of the Cu^{2+}/PDS system showed that homogeneous Cu^{2+} ions were not powerful enough to activate the PDS. As a source of Cu^{2+} ions, we used 20 mg/L of copper(II) sulfate ($CuSO_4$, Merck, Germany), because in this comparison our catalyst dosage was 0.5 g/L and contains 4 mol% of Cu^{2+} in the Cu-BMS catalyst (according to the ICP-OES analysis). The data in Fig. 4a show that 25.5% (within 60 min) of the MB was adsorbed onto the surface of the Cu-BMS particles. The high surface adsorption indicates that the Cu-BMS catalysts have a high specific surface area, which in turn indicates a high number of reaction sites. Therefore, BMS is an excellent support for loading Cu^{2+} ions. Regarding the degradation of MB, the adsorption of Cu-BMS did not reach the required DE% level. In contrast, the Cu-BMS/PDS system increased the DE% of MB to 93.5% within 60 min. The Fig. S2 displays the UV–Vis spectra of MB degradation at various times during the degradation process. The absorbance peak of MB was observed in the range of 500–700 nm, representing the heteropoly aromatic linkage (involving chromophore and auxochrome ($-CH_3$)) [53], with its maximum at $\lambda = 664$ nm, that absorbance was monitored during the MB degradation process. In addition, the catalytic efficacy of Cu-BMS with varying amount of copper (1%, 2%, and 4%) was examined, and the findings are illustrated in Fig. S3. The increase in the copper content in the BMS structure resulted in an increase in the DE %.

To determine the reaction rate constant (k) of MB degradation, pseudo-first order kinetics was applied (Eq. (5)), and a linear fit was performed between $\ln(A_0/A_t)$ and time, where A_0 and A_t are the initial and time-related MB absorption, respectively [54].

$$ln{A_0}/{A_t} = kt \quad (5)$$

The data pertaining to the pre-equilibrium stage (up to 40 min) are described by Eq. (5). Linear plots representing these data are shown in Fig. 4b. From the figure, it can be observed that the rate constant $k_{Cu\text{-}BMS/PDS}$ (0.0641 min^{-1}) is approximately 8 times greater than $k_{Cu\text{-}BMS}$ (0.0077 min^{-1}), almost 17 times greater than $K^{2+}_{Cu/PDS}$ (0.0036 min^{-1}), and almost 20 times greater than k_{PDS} (0.0031 min^{-1}). The higher rate constant of Cu-BMS/PDS compared to that of the other systems indicates its potential as a more effective catalyst for the degradation of MB. The results indicate that the Cu-BMS catalyst can activate PDS and accelerate the degradation of MB. Furthermore, it was observed that the Cu-BMS catalyst exhibited a higher level of reactivity in terms of the degradation rate constant during the activation of PDS compared to some of the catalysts reported in the literature (Table 2).

3.3. Effect of the operating parameters on DE%

3.3.1. Cu-BMS catalyst dosage

Owing to economic considerations, it is important to use an appropriate dosage of the catalyst in the degradation reactions [55]. An investigation of the effect of Cu-BMS dosage on the DE% of MB is shown in Fig. 5a. The DE% of MB increased steadily as the Cu-BMS catalyst dosage was increased until it reached 93.5% at 0.5 g/L catalysts. A higher catalyst dosage enhances PDS activation sites, resulting in increased $SO_4^{\bullet-}$ generation and higher DE% [56]. However, increasing the Cu-BMS dosage from 0.5 to 1.0 g/L did not have a significant effect on DE% (97.3% within 60 min). This could possibly be explained by the fact that the adsorption of persulfate (2 g/L) for activation reached equilibrium when the Cu-BMS dosage was at 0.5 g/L [57].

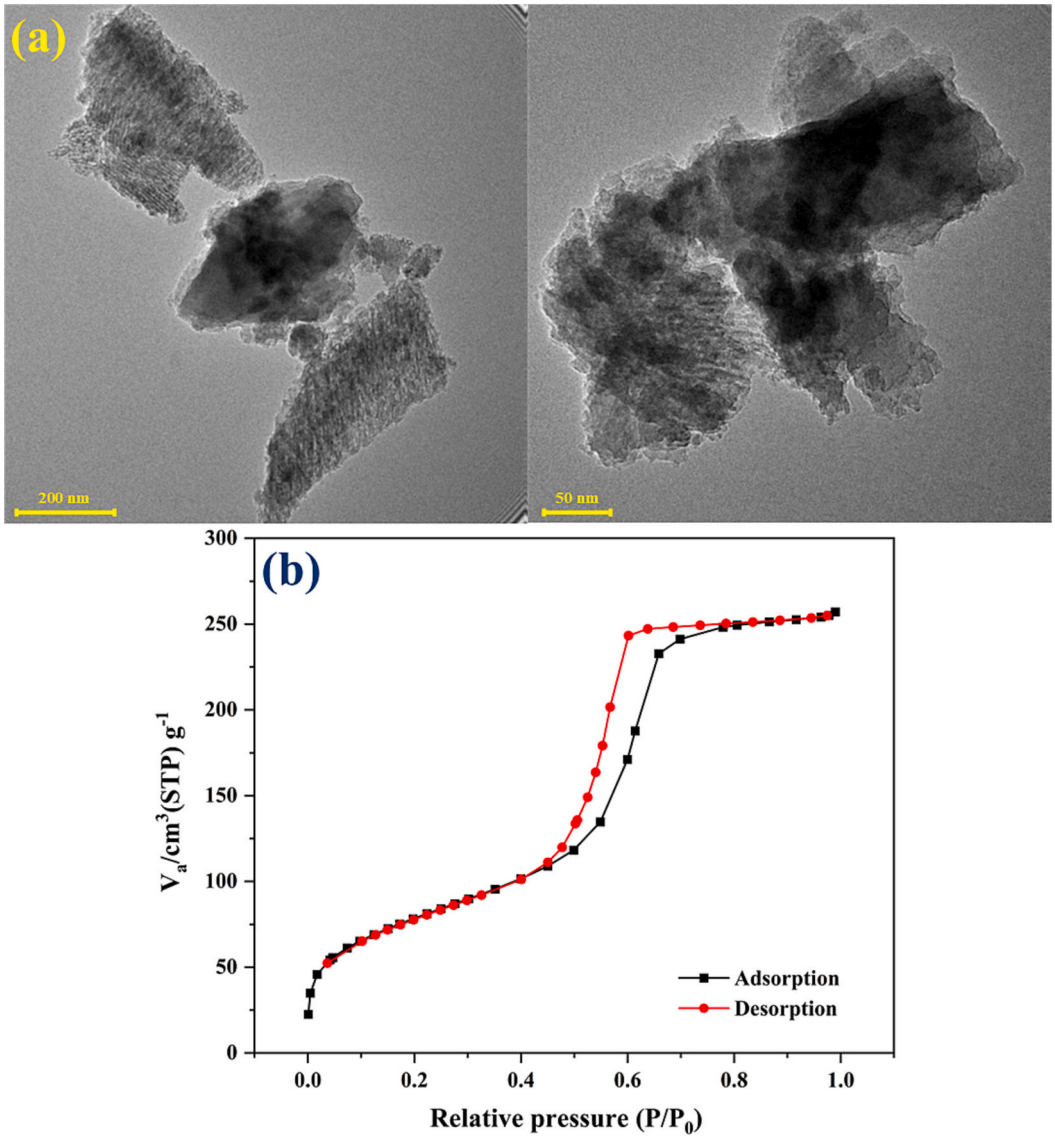

Fig. 3. (a) TEM images at different magnification and (b) Nitrogen adsorption isotherm of the Cu-BMS particles.

3.3.2. PDS dosage

In Fig. 5b, the catalytic activity of the Cu-BMS catalyst was investigated at different concentrations of PDS (0.5, 1.0, 2.0, 3.0, and 4.0 g/L) in the presence of a fixed quantity of catalyst (0.5 g/L) and MB (100 mg/L). By increasing the PDS dosage from 0.5 to 3.0 g/L, the DE% increased from 63.5% to 95.6% within 60 min. At high PDS dosages, high concentrations of active radicals facilitated the oxidation of contaminant molecules (Fig. S4). Nonetheless, DE% decreased significantly with a further increase in the PDS dosage (4.0 g/L). In the presence of high dosages of PDS, $SO_4^{\bullet-}$ can react with PDS to form less active radicals, as shown in Eq. (6) and the chain-termination reaction between $SO_4^{\bullet-}$ radicals (Eq. (7)) may hinder the oxidation of MB [58,59].

$$SO_4^{\bullet-} + S_2O_8^{2-} \rightarrow S_2O_8^{\bullet-} + SO_4^{2-} \quad (6)$$

$$SO_4^{\bullet-} + SO_4^{\bullet-} \rightarrow S_2O_8^{2-} \quad (7)$$

3.3.3. Initial pH

It is well known that the DE% of organic contaminants can be significantly affected by adjusting the solution's initial pH. We investigated the DE% of MB at five different pH levels (2.5, 4.5, 6.5, 8.5, and 10.5), and the results are summarized in Fig. 5c. Solutions of NaOH (0.1 mol/L) and H_2SO_4 (0.1 mol/L) were used to adjust the initial pH of the pollutant solution. As shown in Fig. 5c, the acidic environment improved the DE% of MB, whereas the alkaline environment had a negative impact. The higher DE% under acidic conditions was due to the generation of more $SO_4^{\bullet-}$ radicals, according to the reactions given in Eqs. (8–11) [56,60]. Furthermore, at high pH levels, high concentrations of OH^- can scavenge $SO_4^{\bullet-}$ (Eq. (12)) [61].

$$S_2O_8^{2-} + H^+ \rightarrow HS_2O_8^- \quad (8)$$

$$HS_2O_8^- \rightarrow SO_4^{\bullet-} + SO_4^{2-} + H^+ \quad (9)$$

$$SO_4^{\bullet-} + H_2O \rightarrow SO_4^{2-} + OH^{\bullet} + H^+ \quad (10)$$

$$SO_4^{2-} + OH^{\bullet} + H^+ \rightarrow SO_4^{\bullet-} + H_2O \quad (11)$$

$$SO_4^{\bullet-} + OH^- \rightarrow SO_4^{2-} + OH^{\bullet} \quad (12)$$

3.3.4. Initial MB concentration

The degradation of MB at different initial concentrations (50, 100, 200, and 400 mg/L) was also investigated in the presence of a fixed quantity of catalyst (0.5 g/L) and PDS (2.0 g/L) at pH 6.5. By increasing

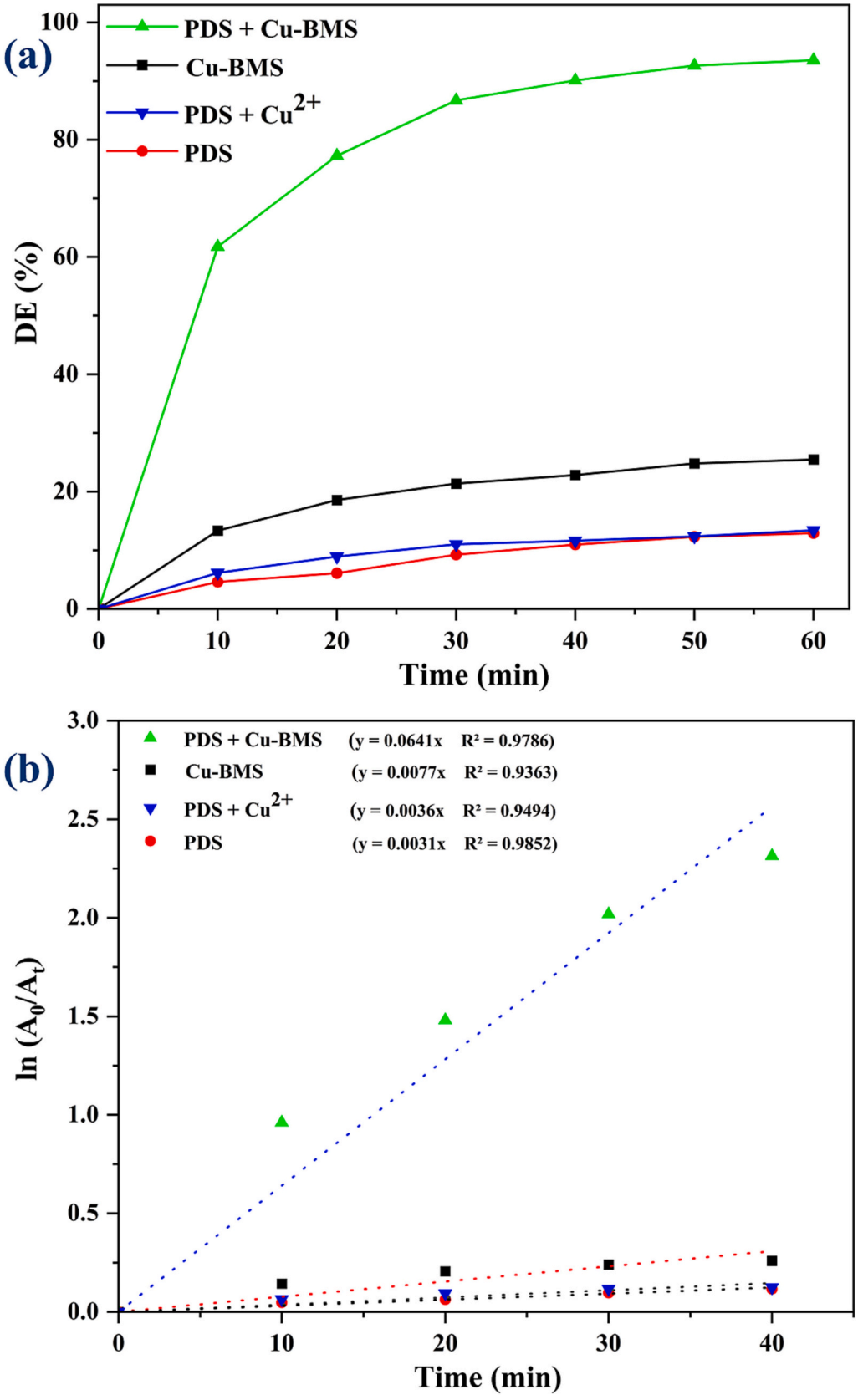

Fig. 4. (a) DE% of MB; and (b) the pseudo-first-order kinetic rate plot for different systems (Parameters: [Cu-BMS] = 0.5 g/L, [PDS] = 2.0 g/L, [MB] = 100 mg/L and pH = 6.5 (original pH of MB)).

Table 2
Degradation efficiency of organic molecules during activation of persulfate with different catalysts.

Catalyst	Conditions	DE (%) - Time (min)	Ref.
Mesoporous silica spheres	[MB] = 50 mg/L, [PDS] = 3.7 mM, [Catalyst] = 1 g/L, pH = 5	90% - 60	[59]
Fe–Co-SBA	[Orange II] = 70 mg/L, [PDS] = 20 mM, [Catalyst] = 1 g/L, pH = 3–7	>80% - 120	[73]
α-MnO_2/ Palygorskite	[RhB] = 20 mg/L, [PMS] = 0.9 mM, [Catalyst] = 0.1 g/L, pH < 5.5	~100% - 300	[74]
CuO/Fe_2O_3/ $CuFe_2O_4$	[Levofloxacin] = 10 mg/L, [PDS] = 7 mM, [Catalyst] = 0.5 g/L, pH = 6.4	75.5% - 120	[75]
Cu/ZSM5	[RhB] = 50 mg/L, [PMS] = 5 mM, [Catalyst] = 1 g/L, pH = 7	99% - 60	[76]
Cu-BMS	[MB] = 100 mg/L, [PDS] = 10 mM, [Catalyst] = 0.5 g/L, pH = 6.5	93% - 60	This study

the initial concentration of MB from 50 to 400 mg/L within 60 min, the DE% decreased from almost 100% to 44.6% (Fig. 5d). A constant number of active radicals were generated under specific operating conditions, such as the catalyst dosage, PDS dosage, and reaction time. Hence, insufficient active radicals would be present in the presence of a high concentration of MB molecules, resulting in a low DE%. Furthermore, when MB is present at high concentrations, the active sites of the catalyst can be clogged with MB molecules, which can reduce the effectiveness of the catalyst in degrading MB molecules [62].

3.3.5. Reaction temperature

The influence of different temperatures (25, 45, and 65 °C) on the Cu-BMS/PDS system is shown in Fig. 6a. The degradation of MB exhibited a consistent upward trend as the temperature increased. For example, the decomposition of MB increased from 61% to 97% after 10 min of reaction time as the temperature rose from 25 °C to 65 °C. This demonstrates that PDS was also activated by heat producing reactive sulfate radical species active in MB degradation process [63].

3.3.6. Stability

Catalyst stability and reusability play major roles in the cost-effectiveness of heterogeneous water treatment. Therefore, twelve consecutive MB degradation tests were performed on the Cu-BMS catalyst, and the results are shown in Fig. 6b. In the first cycle, 93.5% of MB was degraded within 60 min. During the fourth, eighth, and twelfth cycles, the MB DE% decreased to 84.3%, 75.7%, and 70.4%,

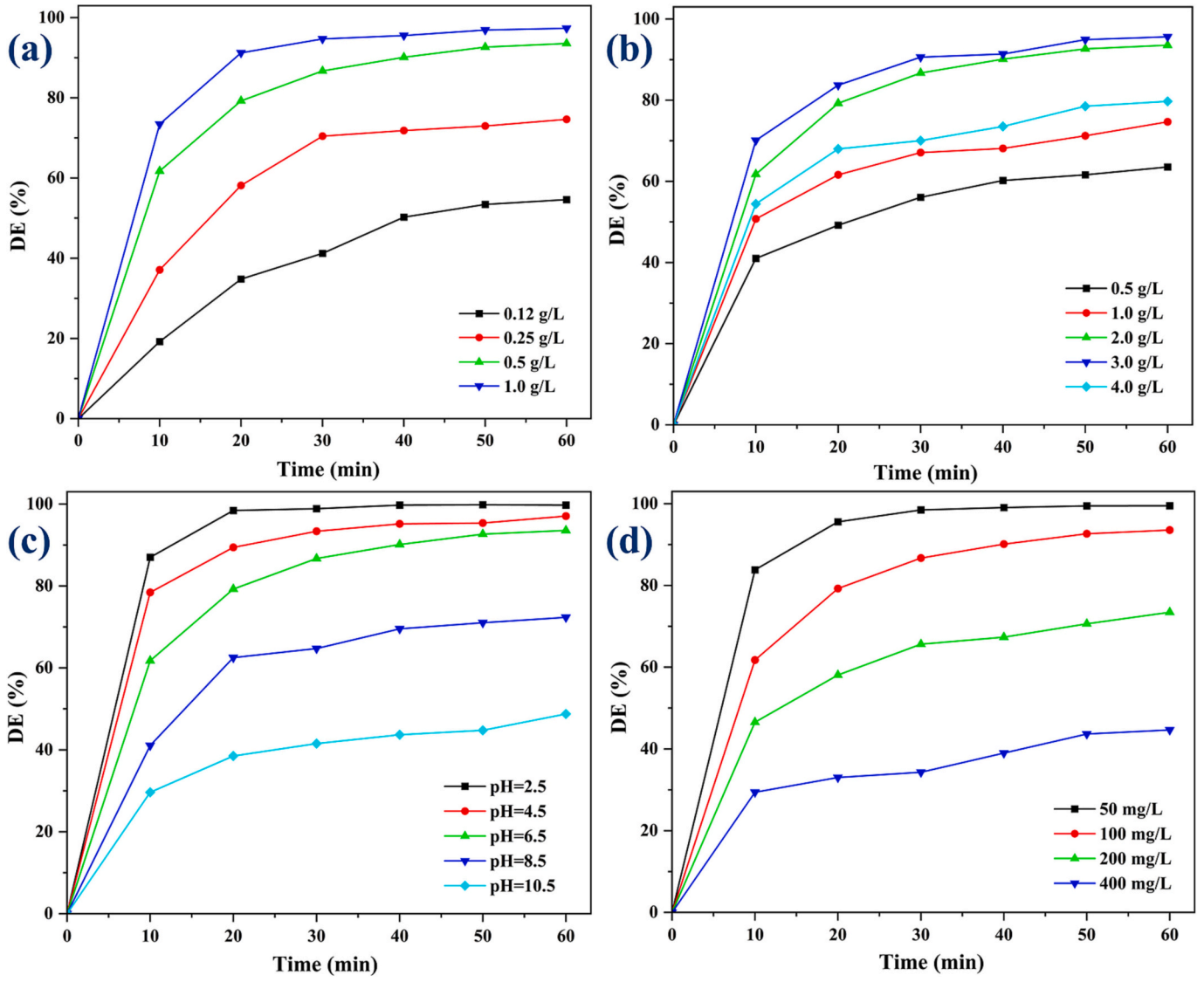

Fig. 5. Effect of (a) Cu-BMS catalyst dosage, (b) PDS dosage, (c) initial pH, and (d) initial MB concentration on DE% in the Cu-BMS/PDS system (Parameters: [Cu-BMS] = 0.5 g/L, [PDS] = 2.0 g/L, [MB] = 100 mg/L, and pH = 6.5).

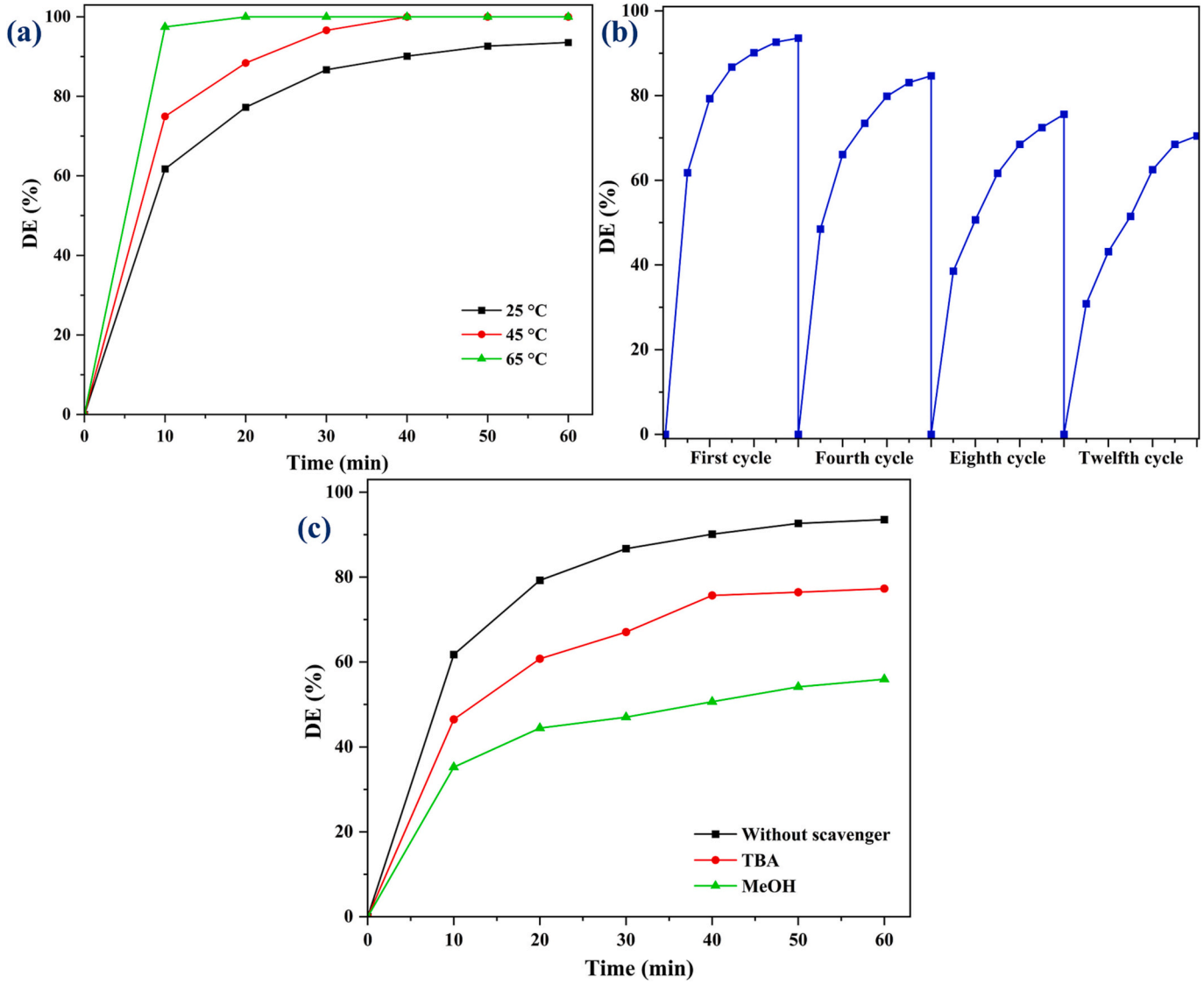

Fig. 6. (a) Effect of temperature on DE% in the Cu-BMS/PDS system; (b) MB degradation of Cu-BMS/PDS system in the first, fourth, eighth, and twelfth cycles; and (c) effect of reactive radical species scavengers on the DE% (Parameters: [Cu-BMS] = 0.5 g/L, [PDS] = 2.0 g/L, [MB] = 100 mg/L and pH = 6.5).

respectively. The Cu-BMS catalyst maintained an acceptable DE% (70%) even after the twelfth cycle of degradation tests, indicating its durability and reusability. Additionally, structural stability of Cu-BMS catalyst was examined by XRD (Fig. S5) and FESEM (Fig. S6) analysis after twelve times use. The comparable morphology and XRD pattern observed in the utilized catalyst and the pristine Cu-BMS provides evidence for the structural integrity and stability of the Cu-BMS catalyst after several time usage. This indicates that the Cu-BMS synthesized in this study exhibits a notable level of structural stability and satisfactory reusability when employed in the degradation of organic contaminants within the Cu-BMS/PDS system.

The concentration of Cu leaching (0.5 g/L Cu-BMS in 100 mL solution with a pH of 6.5) was measured by ICP-OES. The results showed that the Cu concentrations in the above-mentioned tests were 0.105 mg/L (first run), 0.088 mg/L (fourth run), 0.026 mg/L (eighth run), and 0.017 mg/L (twelfth run). The World Health Organization (WHO) and the European Water Quality Directive recommend a Cu concentration below 2.0 mg/L in drinking water. Therefore, the concentration of Cu leached from the catalyst was lower than the standard Cu concentration [64].

3.4. Investigation of the reactive radical species

The EPR spin trapping technique was applied to confirm the formation of reactive radical species as their paramagnetic intermediates with spin trapping agents. DMPO (5,5-dimethyl-1-pyrroline N-oxide), as in many studies often applied, was used as a spin trapping agent of the $SO_4^{\bullet-}$ and $HO^{\bullet}$ radicals, and TMPO was used to detect the singlet oxygen species $^1O_2$. In the system Cu-BMS/PDS/DMPO formation of two spin-adducts was identified (Fig. S7), the $^{\bullet}$DMPO-OH (spin Hamiltonian parameters: $a_N = 1.504$ mT, $a_H^{\beta} = 1.459$ mT; g = 2.0057, $c_{rel} = 52\%$) and the signal of the $^{\bullet}$DMPO-SO_4^- adduct (spin Hamiltonian parameters: $a_N = 1.370$ mT, $a_H^{\beta} = 1.007$ mT, $a_H^{\gamma 1} = 0.142$ mT, $a_H^{\gamma 2} = 0.076$ mT; g = 2.0057, $c_{rel} = 48\%$). The EPR signal of the $^{\bullet}$DMPO-SO_4^- adduct was weaker than that of $^{\bullet}$DMPO-OH, and the intensity of $^{\bullet}$DMPO-OH signal increased with time. This is because the capture efficiency of DMPO is higher for $HO^{\bullet}$ radicals than for $SO_4^{\bullet-}$ [65], and additionally, $^{\bullet}$DMPO-SO_4^- adduct can undergo rapid nucleophilic substitution to form hydroxyl radical adduct $^{\bullet}$DMPO-OH which is monitored [66]. Also, sulfate radicals can transfer into hydroxyl radicals at neutral pH, according to Eq. (10). The same species ($^{\bullet}$DMPO-SO_4^- $c_{rel} = 44\%$, $^{\bullet}$DMPO-OH $c_{rel} = 56\%$), however in lower concentration, were observed also in reaction

system PDS/DMPO without the presence of the catalyst. As recently reported by L. Wang et al. [67] in their detailed study, this is due to the direct oxidation of the DMPO agent under highly oxidizing conditions; PDS dosage and reaction time play an important role. Their study showed, that at zero reaction time no radical signal was detected, but even after 2 or 5 min the signal of $^{\bullet}$DMPO-OH adduct was clearly observed in sufficiently high intensity especially at higher concentration of DMPO (over 50 mmol/L) in the PDS/DMPO system. Therefore, the selecting the proper spin traps and especially performing careful control tests are necessary in the study of catalytic oxidation mechanism under highly oxidizing conditions like in the case of PDS. The higher signal intensity of the species in the system Cu-BMS/PDS/DMPO, however points to the generation of the $SO_4^{\bullet-}$ and $HO^{\bullet}$ radicals by the Cu-BMS catalyst. The generation of singlet oxygen $^1O_2$ was examined by applying sterically hindered amine 4-oxo-2,2,6,6-tetramethylpiperidone (TMPO). However only weak EPR signal of stable nitroxide 4-oxo-2,2,6,6-tetramethylpiperidine 1-oxyl (TEMPO) with characteristic three-line spectrum (data not shown) was observed in both reaction systems (Cu-BMS/PDS/TMPO/air and PDS/TMPO/air) which indicates only limited formation of the $^1O_2$ under given experimental conditions.

To identify the contributions of different reactive radicals in the Cu-BMS/PDS system, we performed active radical quenching studies. MeOH and tert-butanol (TBA) were used to quench the active radicals (Fig. 6c). MeOH was selected as a scavenger for $SO_4^{\bullet-}$ ($k = 1.6–7.7 \times 10^7$ 1/M.s) and $HO^{\bullet}$ ($k = 1.2–2.8 \times 10^9$ 1/M.s) radicals. Additionally, TBA is a selective scavenger only for $HO^{\bullet}$ ($k = 3.8–7.6 \times 10^8$ 1/M.s) [7,52,68]. The use of MeOH (0.5 mol/L) as a scavenger for both $SO_4^{\bullet-}$ and $HO^{\bullet}$ radicals led to a significant decrease in DE% (from 93.5% to 55.9%), indicating a significant contribution of these radicals to the MB degradation reactions. In contrast, TBA (0.5 mol/L), which selectively scavenges only $HO^{\bullet}$ radicals, led to a lower decrease in DE% (from 93.5% to 77.3%), indicating a relatively smaller contribution of $HO^{\bullet}$ radicals to the reactions. These results suggest that $SO_4^{\bullet-}$ radicals may play a larger role in the degradation of MB in the Cu-BMS/PDS system.

3.5. MB degradation mechanism

The schematic representation of the mechanism and reaction pathway in the PDS system is provided in Fig. 7, and it is based on the literature experimental data gained from MB degradation [69–72]. The first stage of MB degradation involves the reaction with $HO^{\bullet}$ and $SO_4^{\bullet-}$ radicals, leading to the conversion of C=N–C and C–S^+=C bonds into C–NH–C and C–SH(=O)$_2$–C. This process results in the opening of the core aromatic ring that contains both nitrogen and sulfur heteroatoms. As depicted in Fig. 7, the reaction generates intermediate compounds through the destruction of benzene rings. Finally, uncomplicated, minimally harmful organic acids (like oxalic acid and acetic acid) or mineralized inorganic compounds (like water, carbon dioxide, nitrate,

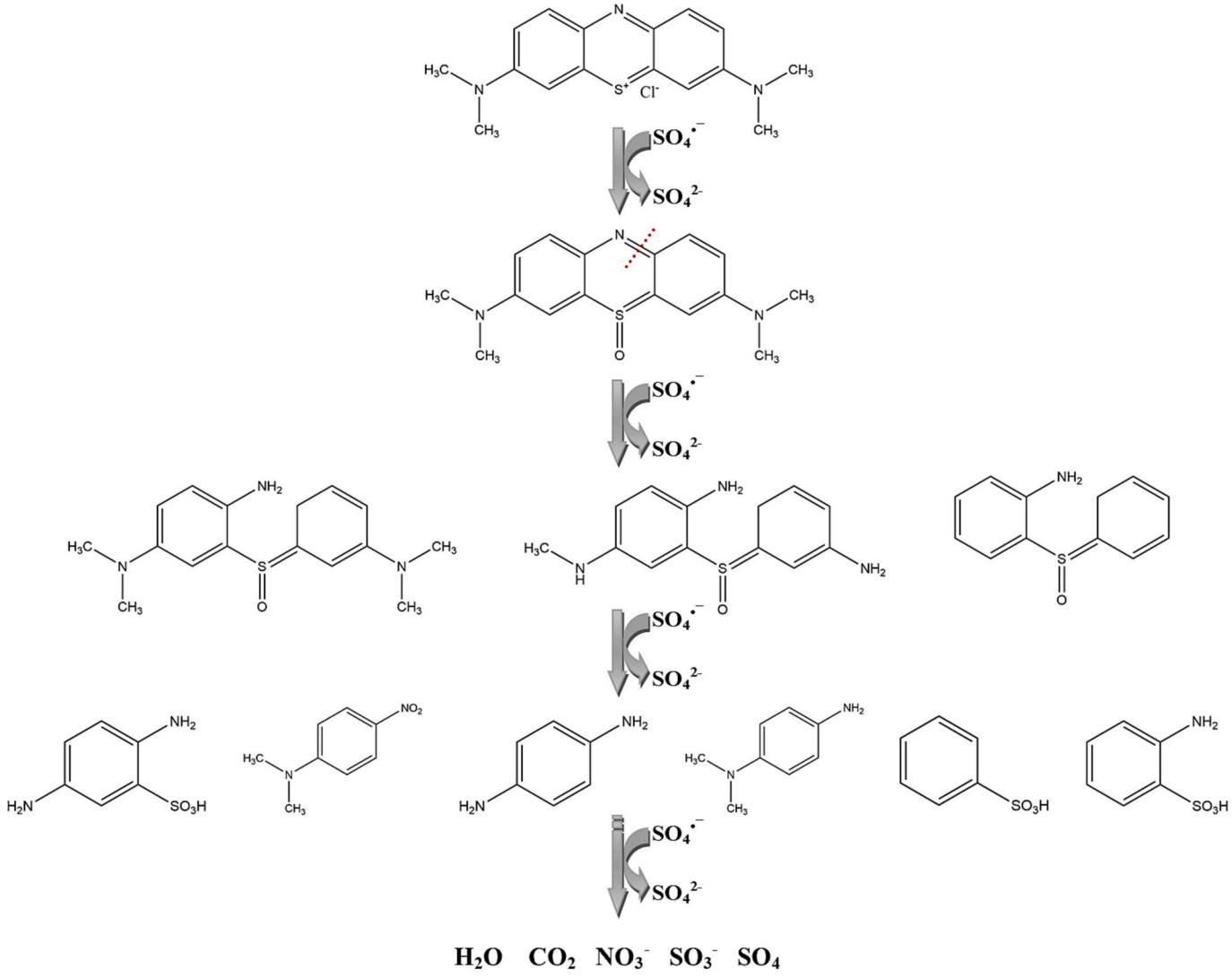

Fig. 7. Proposed mechanism for the decomposition of MB in a solution of the activated persulfate.

sulfate, and sulfite) are generated.

4. Conclusion

The EISA sol-gel procedure was used to synthesize mesoporous Cu-BMS (SiO_2-CaO-CuO-P_2O_5) particles containing 4 mol% CuO. High surface areas and regular mesopores were observed in the prepared Cu-BMS, which improved its catalytic activity. Cu-BMS was used to activate PDS as a heterogeneous catalyst for the oxidation of MB dye. A comparison between the Cu-BMS/PDS, Cu^{2+}/PDS, Cu-BMS (adsorption), and PDS systems showed that Cu-BMS catalysts are capable of activating PDS with high catalytic capabilities, resulting in a higher degradation efficiency (93.5% within 60 min) and a faster degradation rate (0.0641 min^{-1}) than Cu^{2+}/PDS. The DE% was affected by the Cu-BMS dosage, PDS amount, pH level, and MB concentration in the Cu-BMS/PDS system. Cu-BMS was still able to effectively degrade 70.4% in 60 min of MB after twelve cycles. In reactive radical quenching tests, $SO_4^{\bullet-}$, and $^{\bullet}OH$ were found to participate in the catalytic degradation of MB, while the most responsible radical was $SO_4^{\bullet-}$. Based on the findings of this study, mesoporous silica particles are potentially useful support materials for wastewater treatment.

CRediT authorship contribution statement

Saeed Sajjadi: Conceptualization, Data curation, Formal analysis, Investigation, Writing – original draft, Writing – review & editing. **Akrity Anand:** Conceptualization, Data curation, Formal analysis, Investigation. **Ana M. Beltrán:** Investigation, Validation, Writing – review & editing. **Dana Dvoranová:** Data curation, Formal analysis, Investigation. **Aldo R. Boccaccini:** Supervision, Writing – review & editing. **Dagmar Galusková:** Supervision, Validation, Writing – review & editing. **David Jaška:** Data curation, Formal analysis, Investigation. **Róbert Klement:** Conceptualization, Data curation, Formal analysis, Investigation, Writing – original draft, Writing – review & editing.

Declaration of Competing Interest

The authors declare that they have no known competing financial interests or personal relationships that could have appeared to influence the work reported in this paper.

Data availability

Data will be made available on request.

Acknowledgement

This item is a part of dissemination activities of project FunGlass. This project has received funding from the European Union's Horizon 2020 Research and Innovation Programme under grant agreement No 739566. Dana Dvoranová thanks for the financial support to Scientific Grant Agency of the Slovak Republic (VEGA 1/0064/21). The authors would like to express their gratitude to Dr. Hana Kaňková, Lenka Buňová and Dr. Kamalan Mosas (FunGlass – Centre for Functional and Surface Functionalized Glass, Alexander Dubček University of Trenčín, Slovakia) for conducting ICP-OES measurements and for recording the XPS spectra and helpful discussion. They would also like to thank Lukáš Münster and Jakub Ševčík (Centre of Polymer Systems, Tomas Bata University, Zlín, Czech Republic) for performing the BET analysis. Additionally, the authors extend their thanks to the central facilities of Universidad de Sevilla (CITIUS) for providing access to the TEM.

Appendix A. Supplementary data

Supplementary data to this article can be found online at https://doi.org/10.1016/j.catcom.2023.106833.

References

[1] Z. Mengting, T.A. Kurniawan, S. Fei, T. Ouyang, M.H.D. Othman, M. Rezakazemi, S. Shirazian, Applicability of $BaTiO_3$/graphene oxide (GO) composite for enhanced photodegradation of methylene blue (MB) in synthetic wastewater under UV–vis irradiation, Environ. Pollut. 255 (2019) 113182, https://doi.org/10.1016/J.ENVPOL.2019.113182.

[2] T.A. Kurniawan, Z. Mengting, D. Fu, S.K. Yeap, M.H.D. Othman, R. Avtar, T. Ouyang, Functionalizing TiO_2 with graphene oxide for enhancing photocatalytic degradation of methylene blue (MB) in contaminated wastewater, J. Environ. Manag. 270 (2020) 110871, https://doi.org/10.1016/J.JENVMAN.2020.110871.

[3] X. Liu, H. Pang, X. Liu, Q. Li, N. Zhang, L. Mao, M. Qiu, B. Hu, H. Yang, X. Wang, Orderly porous covalent organic frameworks-based materials: superior adsorbents for pollutants removal from aqueous solutions, Innovation. 2 (2021) 100076, https://doi.org/10.1016/J.XINN.2021.100076.

[4] L. Yao, H. Yang, Z. Chen, M. Qiu, B. Hu, X. Wang, Bismuth oxychloride-based materials for the removal of organic pollutants in wastewater, Chemosphere. 273 (2021) 128576, https://doi.org/10.1016/J.CHEMOSPHERE.2020.128576.

[5] C. Yin, Y. Liu, X. Kang, X. Li, Synergistic degradation of tetracycline by CDs decorated g-C_3N_4 under LED light irradiation combined with the persulfate-based advanced oxidation process, Appl. Catal. A Gen. 636 (2022) 118571, https://doi.org/10.1016/J.APCATA.2022.118571.

[6] B.O. Orimolade, A.O. Idris, U. Feleni, B. Mamba, Peroxymonosulfate assisted photoelectrocatalytic degradation of pharmaceuticals at a FTO-Bi_2WO_6 electrode: mechanism and kinetics studies, Catal. Commun. 169 (2022) 106481, https://doi.org/10.1016/J.CATCOM.2022.106481.

[7] A. Jawad, J. Lang, Z. Liao, A. Khan, J. Ifthikar, Z. Lv, S. Long, Z. Chen, Z. Chen, Activation of persulfate by CuO_x@co-LDH: a novel heterogeneous system for contaminant degradation with broad pH window and controlled leaching, Chem. Eng. J. 335 (2018) 548–559, https://doi.org/10.1016/J.CEJ.2017.10.097.

[8] D. Tian, H. Zhou, H. Zhang, P. Zhou, J. You, G. Yao, Z. Pan, Y. Liu, B. Lai, Heterogeneous photocatalyst-driven persulfate activation process under visible light irradiation: from basic catalyst design principles to novel enhancement strategies, Chem. Eng. J. 428 (2022) 131166, https://doi.org/10.1016/J.CEJ.2021.131166.

[9] Z.Y. Choong, K.Y.A. Lin, G. Lisak, T.T. Lim, W. da Oh, Multi-heteroatom-doped carbocatalyst as peroxymonosulfate and peroxydisulfate activator for water purification: a critical review, J. Hazard. Mater. 426 (2022) 128077, https://doi.org/10.1016/J.JHAZMAT.2021.128077.

[10] Y. Ding, K. Cui, X. Liu, C.X. Li, Z. Guo, M. Cui, Y. Chen, Axial g-C3N4 coordinated iron(III) phthalocyanine mediated ultra-efficient peroxymonosulfate activation for high-valent iron species generation, Appl. Catal. A Gen. 641 (2022) 118679, https://doi.org/10.1016/J.APCATA.2022.118679.

[11] H. Jin, L. Zhu, X. Xu, X. Yu, X. Qu, Z. Liu, Y. Yang, Y. Gao, Q. Wei, Synergistic pollutant degradation by Ag_3PO_4/Fe_3O_4/graphene oxide visible light–persulfate coupled system: mechanism elucidation and performance optimization, Catal. Commun. 177 (2023) 106643, https://doi.org/10.1016/J.CATCOM.2023.106643.

[12] Y. Chen, J. Yan, D. Ouyang, L. Qian, L. Han, M. Chen, Heterogeneously catalyzed persulfate by CuMgFe layered double oxide for the degradation of phenol, Appl. Catal. A Gen. 538 (2017) 19–26, https://doi.org/10.1016/J.APCATA.2017.03.020.

[13] K. Chen, L. Zhou, W. Xu, Z. Hu, M. Jia, L. Liu, A novel way of activating peroxysulfate by zero-valent copper and ferroferric oxide co-modified biochar to remove bisphenol A in aqueous solution: performance, mechanism and potential toxicity, Appl. Catal. A Gen. 636 (2022) 118575, https://doi.org/10.1016/J.APCATA.2022.118575.

[14] Y. Ding, L. Fu, X. Peng, M. Lei, C. Wang, J. Jiang, Copper catalysts for radical and nonradical persulfate based advanced oxidation processes: certainties and uncertainties, Chem. Eng. J. 427 (2022) 131776, https://doi.org/10.1016/J.CEJ.2021.131776.

[15] A. Jawad, K. Zhan, H. Wang, A. Shahzad, Z. Zeng, J. Wang, X. Zhou, H. Ullah, Z. Chen, Z. Chen, Tuning of persulfate activation from a free radical to a nonradical pathway through the incorporation of non-redox magnesium oxide, Environ. Sci. Technol. 54 (2020) 2476–2488, https://doi.org/10.1021/acs.est.9b04696.

[16] S. Wacławek, H.V. Lutze, K. Grübel, V.V.T. Padil, M. Černík, D.D. Dionysiou, Chemistry of persulfates in water and wastewater treatment: a review, Chem. Eng. J. 330 (2017) 44–62, https://doi.org/10.1016/J.CEJ.2017.07.132.

[17] H. Li, J. Tian, F. Xiao, R. Huang, S. Gao, F. Cui, S. Wang, X. Duan, Structure-dependent catalysis of cuprous oxides in peroxymonosulfate activation via nonradical pathway with a high oxidation capacity, J. Hazard. Mater. 385 (2020) 121518, https://doi.org/10.1016/J.JHAZMAT.2019.121518.

[18] L. Wang, H. Xu, N. Jiang, Z. Wang, J. Jiang, T. Zhang, Trace cupric species triggered decomposition of Peroxymonosulfate and degradation of organic pollutants: cu(III) being the primary and selective intermediate oxidant, Environ. Sci. Technol. 54 (2020) 4686–4694, https://doi.org/10.1021/acs.est.0c00284.

[19] W. da Oh, T.T. Lim, Design and application of heterogeneous catalysts as peroxydisulfate activator for organics removal: an overview, Chem. Eng. J. 358 (2019) 110–133, https://doi.org/10.1016/J.CEJ.2018.09.203.

[20] D. Li, Q. Zhao, H. Li, M. Long, Synergetic effect of photocatalysis and peroxymonosulfate activated by ZnM_2O_4/SBA–15 (M = Fe and Mn) for enhanced degradation efficiency of doxycycline hydrochloride under visible light irradiation, Mater Today Commun. 31 (2022) 103315, https://doi.org/10.1016/J.MTCOMM.2022.103315.

[21] L. Lopez, V. Montes, H. Kušar, S. Cabrera, M. Boutonnet, S. Järås, Syngas conversion to ethanol over a mesoporous Cu/MCM-41 catalyst: effect of K and Fe promoters, Appl. Catal. A Gen. 526 (2016) 77–83, https://doi.org/10.1016/J.APCATA.2016.08.006.

[22] W. Fu, C. Yin, Y. Feng, L. Zhang, F. Cheng, Z. Fang, C. Zhu, T. Tang, Synergistic catalysis of the Brönsted acid and highly dispersed Cu on the mesoporous Beta zeolite in the intermolecular aminoazidation of styrene, Appl. Catal. A Gen. 609 (2021) 117907, https://doi.org/10.1016/J.APCATA.2020.117907.
[23] M. Pei, X. Luo, Q. Tang, N. Huang, L. Wang, The application research on Cu-Al@SBA-15 bimetallic synergistic effect in the C-X bond sequential assembly, Catal. Commun. 172 (2022) 106548, https://doi.org/10.1016/J.CATCOM.2022.106548.
[24] A.L. Petre, J.B. Carbajo, R. Rosal, E. Garcia-Calvo, J.A. Perdigón-Melón, CuO/SBA-15 catalyst for the catalytic ozonation of mesoxalic and oxalic acids. Water matrix effects, Chem. Eng. J. 225 (2013) 164–173, https://doi.org/10.1016/J.CEJ.2013.03.071.
[25] S. Karthikeyan, M.P. Pachamuthu, M.A. Isaacs, S. Kumar, A.F. Lee, G. Sekaran, Cu and Fe oxides dispersed on SBA-15: a Fenton type bimetallic catalyst for N, N-diethyl-p-phenyl diamine degradation, Appl. Catal. B. 199 (2016) 323–330, https://doi.org/10.1016/J.APCATB.2016.06.040.
[26] A. Šuligoj, A. Ristić, G. Dražić, A. Pintar, N.Z. Logar, N.N. Tušar, Bimetal Cu-Mn porous silica-supported catalyst for Fenton-like degradation of organic dyes in wastewater at neutral pH, Catal. Today 358 (2020) 270–277, https://doi.org/10.1016/J.CATTOD.2020.03.047.
[27] O.B. Ayodele, O.S. Togunwa, Catalytic activity of copper modified bentonite supported ferrioxalate on the aqueous degradation and kinetics of mineralization of direct blue 71, acid green 25 and reactive blue 4 in photo-Fenton process, Appl. Catal. A Gen. 470 (2014) 285–293, https://doi.org/10.1016/J.APCATA.2013.11.013.
[28] B.K. Ghosh, S. Hazra, B. Naik, N.N. Ghosh, Preparation of cu nanoparticle loaded SBA-15 and their excellent catalytic activity in reduction of variety of dyes, Powder Technol. 269 (2015) 371–378, https://doi.org/10.1016/J.POWTEC.2014.09.027.
[29] C. Wu, Y. Zhou, M. Xu, P. Han, L. Chen, J. Chang, Y. Xiao, Copper-containing mesoporous bioactive glass scaffolds with multifunctional properties of angiogenesis capacity, osteostimulation and antibacterial activity, Biomaterials. 34 (2013) 422–433, https://doi.org/10.1016/J.BIOMATERIALS.2012.09.066.
[30] S. Stoll, A. Schweiger, EasySpin, a comprehensive software package for spectral simulation and analysis in EPR, J. Magn. Reson. 178 (2006) 42–55, https://doi.org/10.1016/J.JMR.2005.08.013.
[31] X. Li, X. Min, X. Hu, Z. Jiang, C. Li, W. Yang, F. Zhao, In-situ synthesis of highly dispersed cu-Cu_xO nanoparticles on porous carbon for the enhanced persulfate activation for phenol degradation, Sep. Purif. Technol. 276 (2021) 119260, https://doi.org/10.1016/J.SEPPUR.2021.119260.
[32] Y. Liu, W. Guo, H. Guo, X. Ren, Q. Xu, Cu (II)-doped V_2O_5 mediated persulfate activation for heterogeneous catalytic degradation of benzotriazole in aqueous solution, Sep. Purif. Technol. 230 (2020) 115848, https://doi.org/10.1016/J.SEPPUR.2019.115848.
[33] Y. Qiu, J. Zhou, J. Cai, W. Xu, Z. You, C. Yin, Highly efficient microwave catalytic oxidation degradation of p-nitrophenol over microwave catalyst of pristine α-Bi_2O_3, Chem. Eng. J. 306 (2016) 667–675, https://doi.org/10.1016/J.CEJ.2016.06.133.
[34] K. Zheng, A. Solodovnyk, W. Li, O.-M. Goudouri, C. Stähli, S.N. Nazhat, A. R. Boccaccini, Aging time and temperature effects on the structure and bioactivity of gel-derived 45S5 glass-ceramics, J. Am. Ceram. Soc. 98 (2015) 30–38, https://doi.org/10.1111/jace.13258.
[35] I. Cacciotti, M. Lombardi, A. Bianco, A. Ravaglioli, L. Montanaro, Sol–gel derived 45S5 bioglass: synthesis, microstructural evolution and thermal behaviour, J. Mater. Sci. Mater. Med. 23 (2012) 1849–1866, https://doi.org/10.1007/s10856-012-4667-6.
[36] R. Koohkan, T. Hooshmand, M. Tahriri, D. Mohebbi-Kalhori, Synthesis, characterization and in vitro bioactivity of mesoporous copper silicate bioactive glasses, Ceram. Int. 44 (2018) 2390–2399, https://doi.org/10.1016/J.CERAMINT.2017.10.208.
[37] B. Djamila, L.S. Eddine, B. Abderrhmane, A. Nassiba, A. Barhoum, In vitro antioxidant activities of copper mixed oxide (CuO/Cu_2O) nanoparticles produced from the leaves of *Phoenix dactylifera* L, Biomass Convers Biorefin. (2022), https://doi.org/10.1007/s13399-022-02743-3.
[38] C. Wu, B. Chen Wang, Li Quan, Dian Wu, Li Dong, Increasing the oral bioavailability of poorly water-soluble carbamazepine using immediate-release pellets supported on SBA-15 mesoporous silica, Int. J. Nanomedicine (2012) 5807, https://doi.org/10.2147/IJN.S37650.
[39] M. Swadźba-Kwaśny, L. Chancelier, S. Ng, H.G. Manyar, C. Hardacre, P. Nockemann, Facile in situ synthesis of nanofluids based on ionic liquids and copper oxide clusters and nanoparticles, Dalton Trans. 41 (2012) 219–227, https://doi.org/10.1039/C1DT11578B.
[40] Y. Zhang, Q. Zhang, Z. Dong, Liying Wu, J. Hong, Degradation of acetaminophen with ferrous/copperoxide activate persulfate: Synergism of iron and copper, Water Res. 146 (2018) 232–243, https://doi.org/10.1016/J.WATRES.2018.09.028.
[41] C. Heras, S. Sanchez-Salcedo, D. Lozano, J. Peña, P. Esbrit, M. Vallet-Regi, A. J. Salinas, Osteostatin potentiates the bioactivity of mesoporous glass scaffolds containing Zn^{2+} ions in human mesenchymal stem cells, Acta Biomater. 89 (2019) 359–371, https://doi.org/10.1016/J.ACTBIO.2019.03.033.
[42] M. Sarmast Sh, S. George, C.A.B. Dayang Radiah, D. Hoey, N. Abdullah, S. Kamarudin, Synthesis of bioactive glass using cellulose nano fibre template, J. Mech. Behav. Biomed. Mater. 130 (2022) 105174, https://doi.org/10.1016/J.JMBBM.2022.105174.
[43] N. Pajares-Chamorro, X. Chatzistavrou, Bioactive glass nanoparticles for tissue regeneration, ACS Omega. 5 (2020) 12716–12726, https://doi.org/10.1021/acsomega.0c00180.
[44] A. Anand, S. Sengupta, H. Kaňková, A. Švančárková, A.M. Beltrán, D. Galusek, A. R. Boccaccini, D. Galusková, Influence of copper-strontium co-doping on bioactivity, cytotoxicity and antibacterial activity of mesoporous bioactive glass, Gels. 8 (2022) 743, https://doi.org/10.3390/gels8110743.
[45] C. Sanchez, C. Boissière, D. Grosso, C. Laberty, L. Nicole, Design, synthesis, and properties of inorganic and hybrid thin films having periodically organized nanoporosity, Chem. Mater. 20 (2008) 682–737, https://doi.org/10.1021/cm702100t.
[46] T. Kimura, Evaporation-induced self-assembly process controlled for obtaining highly ordered mesoporous materials with demanded morphologies, Chem. Rec. 16 (2016) 445–457, https://doi.org/10.1002/tcr.201500262.
[47] M. Thommes, K. Kaneko, A.V. Neimark, J.P. Olivier, F. Rodriguez-Reinoso, J. Rouquerol, K.S.W. Sing, Physisorption of gases, with special reference to the evaluation of surface area and pore size distribution (IUPAC technical report), pure and applied, Chemistry. 87 (2015) 1051–1069, https://doi.org/10.1515/pac-2014-1117.
[48] A. Svidrytski, D. Hlushkou, M. Thommes, P.A. Monson, U. Tallarek, Modeling the impact of mesoporous silica microstructures on the adsorption hysteresis loop, J. Phys. Chem. C 124 (2020) 21646–21655, https://doi.org/10.1021/acs.jpcc.0c07571.
[49] G. Wang, Y. Ju, Organic shale micropore and mesopore structure characterization by ultra-low pressure N_2 physisorption: experimental procedure and interpretation model, J. Nat. Gas Sci. Eng. 27 (2015) 452–465, https://doi.org/10.1016/J.JNGSE.2015.08.003.
[50] A.R. Rahmani, M. Salari, A. Shabanloo, N. Shabanloo, S. Bajalan, Y. Vaziri, Sono-catalytic activation of persulfate by nZVI-reduced graphene oxide for degradation of nonylphenol in aqueous solution: process optimization, synergistic effect and degradation pathway, J. Environ. Chem. Eng. 8 (2020) 104202, https://doi.org/10.1016/J.JECE.2020.104202.
[51] H. Xie, W. Xu, Enhanced activation of persulfate by Meso-$CoFe_2O_4/SiO_2$ with ultrasonic treatment for degradation of Chlorpyrifos, ACS Omega. 4 (2019) 17177–17185, https://doi.org/10.1021/acsomega.9b01626.
[52] Z. Ansarian, A. Khataee, S. Arefi-Oskoui, Y. Orooji, H. Lin, Ultrasound-assisted catalytic activation of peroxydisulfate on Ti_3GeC_2 MAX phase for efficient removal of hazardous pollutants, Mater Today Chem. 24 (2022) 100818, https://doi.org/10.1016/J.MTCHEM.2022.100818.
[53] Z. Jia, L.B.T. La, W.C. Zhang, S.X. Liang, B. Jiang, S.K. Xie, D. Habibi, L.C. Zhang, Strong enhancement on dye photocatalytic degradation by ball-milled TiO_2: a study of cationic and anionic dyes, J. Mater. Sci. Technol. 33 (2017) 856–863, https://doi.org/10.1016/J.JMST.2017.02.006.
[54] T. Shahwan, S. Abu Sirriah, M. Nairat, E. Boyaci, A.E. Eroğlu, T.B. Scott, K. R. Hallam, Green synthesis of iron nanoparticles and their application as a Fenton-like catalyst for the degradation of aqueous cationic and anionic dyes, Chem. Eng. J. 172 (2011) 258–266, https://doi.org/10.1016/J.CEJ.2011.05.103.
[55] L. Liu, C. Yang, W. Tan, Y. Wang, Degradation of acid red 73 by activated persulfate in a heat/Fe_3O_4@AC system with ultrasound intensification, ACS Omega 5 (2020) 13739–13750, https://doi.org/10.1021/acsomega.0c00903.
[56] S. Ding, J. Wan, Y. Wang, Z. Yan, Y. Ma, Activation of persulfate by molecularly imprinted Fe-MOF-74@SiO_2 for the targeted degradation of dimethyl phthalate: effects of operating parameters and chlorine, Chem. Eng. J. 422 (2021) 130406, https://doi.org/10.1016/J.CEJ.2021.130406.
[57] Y. Liu, W. Guo, H. Guo, X. Ren, Q. Xu, Cu (II)-doped V_2O_5 mediated persulfate activation for heterogeneous catalytic degradation of benzotriazole in aqueous solution, Sep. Purif. Technol. 230 (2020) 115848, https://doi.org/10.1016/J.SEPPUR.2019.115848.
[58] M. Ding, W. Chen, H. Xu, Z. Shen, T. Lin, K. Hu, Q. Kong, G. Yang, Z. Xie, Heterogeneous $Fe_2CoTi_3O_{10}$-MXene composite catalysts: synergistic effect of the ternary transition metals in the degradation of 2,4-dichlorophenoxyacetic acid based on peroxymonosulfate activation, Chem. Eng. J. 378 (2019) 122177, https://doi.org/10.1016/J.CEJ.2019.122177.
[59] S. Liang, Z. Ziyu, J. Han, D. Xiaoyan, Facile synthesis of magnetic mesoporous silica spheres for efficient removal of methylene blue via catalytic persulfate activation, Sep. Purif. Technol. 256 (2021) 117801, https://doi.org/10.1016/J.SEPPUR.2020.117801.
[60] M. Nie, Y. Yang, Z. Zhang, C. Yan, X. Wang, H. Li, W. Dong, Degradation of chloramphenicol by thermally activated persulfate in aqueous solution, Chem. Eng. J. 246 (2014) 373–382, https://doi.org/10.1016/J.CEJ.2014.02.047.
[61] A. Fayyaz, K. Saravanakumar, K. Talukdar, Y. Kim, Y. Yoon, C.M. Park, Catalytic oxidation of naproxen in cobalt spinel ferrite decorated $Ti_3C_2T_x$ MXene activated persulfate system: mechanisms and pathways, Chem. Eng. J. 407 (2021) 127842, https://doi.org/10.1016/J.CEJ.2020.127842.
[62] A.H. Mady, M.L. Baynosa, D. Tuma, J.J. Shim, Heterogeneous activation of peroxymonosulfate by a novel magnetic 3D γ-MnO_2@$ZnFe_2O_4$/rGO nanohybrid as a robust catalyst for phenol degradation, Appl. Catal. B 244 (2019) 946–956, https://doi.org/10.1016/J.APCATB.2018.11.086.
[63] L. Qian, F.D. Kopinke, T. Scherzer, J. Griebel, A. Georgi, Enhanced degradation of perfluorooctanoic acid by heat-activated persulfate in the presence of zeolites, Chem. Eng. J. 429 (2022) 132500, https://doi.org/10.1016/J.CEJ.2021.132500.
[64] J. Ge, Y. Shen, W. Wang, Y. Li, Y. Yang, N-doped carbon dots for highly sensitive and selective sensing of copper ion and sulfide anion in lake water, J. Environ. Chem. Eng. 9 (2021) 105081, https://doi.org/10.1016/J.JECE.2021.105081.
[65] W. Qin, G. Fang, Y. Wang, D. Zhou, Mechanistic understanding of polychlorinated biphenyls degradation by peroxymonosulfate activated with $CuFe_2O_4$ nanoparticles: key role of superoxide radicals, Chem. Eng. J. 348 (2018) 526–534, https://doi.org/10.1016/J.CEJ.2018.04.215.
[66] G.S. Timmins, K.J. Liu, E.J.H. Bechara, Y. Kotake, H.M. Swartz, Trapping of free radicals with direct in vivo EPR detection: a comparison of 5,5-dimethyl-1-pyrroline-N-oxide and 5-diethoxyphosphoryl-5-methyl-1-pyrroline-N-oxide as spin traps

for HO and $SO_4^{\bullet-}$, Free Radic. Biol. Med. 27 (1999) 329–333, https://doi.org/10.1016/S0891-5849(99)00049-0.
[67] L. Wang, Q. Li, Y. Fu, Z. Wang, H. Zhu, M. Sillanpää, Undiscovered spin trapping artifacts in persulfate oxidation processes: implications for identification of hydroxyl or sulfate radicals in water, ACS ES&T Water. 3 (2023) 532–541, https://doi.org/10.1021/acsestwater.2c00554.
[68] G.P. Anipsitakis, D.D. Dionysiou, Radical generation by the interaction of transition metals with common oxidants, Environ. Sci. Technol. 38 (2004) 3705–3712, https://doi.org/10.1021/es035121o.
[69] P. Jia, H. Tan, K. Liu, W. Gao, Synthesis, characterization and photocatalytic property of novel ZnO/bone char composite, Mater. Res. Bull. 102 (2018) 45–50, https://doi.org/10.1016/j.materresbull.2018.02.018.
[70] S. Hadi, E. Taheri, M.M. Amin, A. Fatehizadeh, R.L. Gardas, Empirical modeling and kinetic study of methylene blue removal from synthetic wastewater by activation of persulfate with heterogeneous Fenton-like process, J. Mol. Liq. 328 (2021) 115408, https://doi.org/10.1016/j.molliq.2021.115408.
[71] Q. Sun, S. Huang, Z. Li, D. Su, J. Sun, Synergistic activation of persulfate by heat and cobalt-doped-bimetallic-MOFs for effective methylene blue degradation: synthesis, kinetics, DFT calculation, and mechanisms, J. Environ. Chem. Eng. 11 (2023) 109065, https://doi.org/10.1016/j.jece.2022.109065.
[72] A. Ghauch, A.M. Tuqan, N. Kibbi, S. Geryes, Methylene blue discoloration by heated persulfate in aqueous solution, Chem. Eng. J. 213 (2012) 259–271, https://doi.org/10.1016/j.cej.2012.09.122.
[73] Q. Ji, F. Zhu, Y. Lei, H. Cheng, J. Ma, S. Komarneni, Fe–Co-SBA assisted by visible light can effectively activate $NaHSO_3$ or H_2O_2 for enhanced degradation of Orange II: activation of $NaHSO_3$ versus H_2O_2, Microporous Mesoporous Mater. 315 (2021) 110902, https://doi.org/10.1016/J.MICROMESO.2021.110902.
[74] C. Huang, Y. Wang, M. Gong, W. Wang, Y. Mu, Z.H. Hu, α-MnO_2/Palygorskite composite as an effective catalyst for heterogeneous activation of peroxymonosulfate (PMS) for the degradation of rhodamine B, Sep. Purif. Technol. 230 (2020) 115877, https://doi.org/10.1016/J.SEPPUR.2019.115877.
[75] J. Lyu, M. Ge, Z. Hu, C. Guo, One-pot synthesis of magnetic CuO/Fe_2O_3/$CuFe_2O_4$ nanocomposite to activate persulfate for levofloxacin removal: investigation of efficiency, mechanism and degradation route, Chem. Eng. J. 389 (2020) 124456, https://doi.org/10.1016/J.CEJ.2020.124456.
[76] F. Ji, C. Li, Y. Liu, P. Liu, Heterogeneous activation of peroxymonosulfate by Cu/ZSM5 for decolorization of Rhodamine B, Sep. Purif. Technol. 135 (2014) 1–6, https://doi.org/10.1016/J.SEPPUR.2014.07.050.